

TOWARD A ONE SHOT MULTI-PROJECTOR PROFILOMETRY SYSTEM FOR FULL FIELD OF VIEW OBJECT MEASUREMENT

Stuart Woolford, Ian. S. Burnett

School of Electronic and Computer Engineering, RMIT University

ABSTRACT

In this paper a one-shot method to determine the shape of an object from overlapping cosine fringes projected from multiple projectors is presented. This overcomes the limitation with single projector systems that do not allow imaging the entire object with a single shot. The proposed method projects orthogonal fringe patterns from different projectors and uses Fourier domain filtering to isolate the fringes, which are demodulated using an unscented particle filter. Sources of error are discussed and their effects on the resulting parameter estimation are shown, as well as methods to reduce their impact. The proposed method is tested on simulations and real world objects and it is shown to be effective to isolate interfering fringes and determine the shape of an object.

Index Terms— Multi-View Profilometry, Structured Light Projection, Unscented Particle Filter, Multiple Projector Structured Light

1. INTRODUCTION

Most multi-view techniques have so far focused on imaging single view at a time and connecting the images together. Zheng, Guo et al. [1] used an N step phase shifting method to first image the object, and then employed a multi-view connection technique using quaternion based coordinate transform and multi-aperture overlap scanning technique (MAOST) to connect the views. A similar connection technique was used in [2] where the point cloud of the measured object is transformed into cylindrical coordinate system and connected via MAOST. Virtual cylinders were used in [3] to overcome the problem with complex shapes not being represented correctly with cylindrical transforms. Multiple projector methods were used in [4, 5] for full field of view shape measurement. In [4], parallel colour de-Brujn patterns projected from multiple projectors was used for full object detection, while a similar method was used in [5]. However the method of Furukawa et al. requires overlap of each pattern to form a grid in order to process the patterns. Gai and Su [6] presented a multiple projector profilometry system based on inverse function analysis but this requires knowledge of the shape in question and can't be done blind. A colour scheme was presented in [7, 8] where fringes of different colours are projected from each projector.

Bayesian methods have been employed in the past to determine object shape via optical profilometry. Villa, Servin and Castillo [9] employed shape measurement using regularized filters with a Markov random field as a prior. Recursive Bayesian estimation has been attempted before in interference fringe analysis [10-13]. Gurov, Ermolaeva and Zakhrov [10] used a Kalman filter to analyse low-coherence fringes in an interferometry system, however this method still required phase unwrapping, and was only tested on surfaces with up to 100 μ m. The unscented Kalman

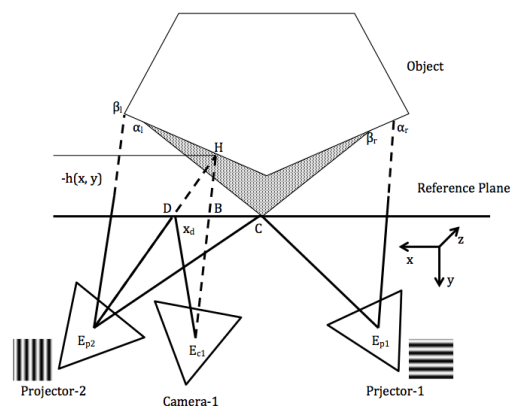


Fig. 1. Setup For The Multi-Projector Profilometry System

filter was used for phase-step interferometry in [14], using a model to estimate the phase and amplitude of an interferometric fringe. This method required phase unwrapping and was only tested for small deformations.

This paper relates to the multi-projector methods in [4, 5], in that each pattern projected from each projector is at right angles to the others. However this paper presents a method where each pattern can be processed individually while allowing for overlap of adjacent patterns thereby reducing the number of projectors required to image the entire object, although it is not fully automatic as the pattern must be selected manually. It also expands on the multi-view one-shot profilometry techniques as opposed to multi-view methods that employ N-ary phase shifting profilometry, which require N shots per view. The proposed method expands on the non-linear filtering methods such as [10-13], however uses an Unscented Particle Filter, which is less sensitive to pixel offset of the input fringe than the standard UKF and increases the estimation accuracy over Bayesian filters by employing the UKF as a proposal distribution.

2. MULTIVIEW PROILOMERTY SETUP

Figure 1 shows the base system setup of the multi-projector profilometry system. Projector-1 (E_p1) and Projector-2 (E_p2) both project onto the object at the same time, with projection field for E_p1 between α_1 and α_2 , and projection field for E_p2 between β_1 and β_2 . In order to capture the full field of view for the object the fringe patterns must overlap crossing at point C. In order to capture the height of the object the fringe pattern from a single projector is projected onto a virtual reference plane to point D. The reference plane is then removed and the fringe pattern is projected

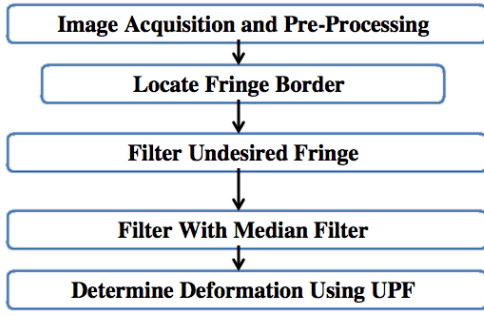


Fig. 2. Block Diagram of the proposed method

onto point H, which is captured by the camera E_c1 . The difference between point D and H (x_d) is the deformation in the fringe pattern caused by the object. In the multi-projector setup the point H lies within the projection fields of both projectors E_p1 and E_p2 . This results in interference between the patterns projected by E_p1 and E_p2 , and any other points captured within the field of view by E_c1 lying between α_1 and β_1 . To efficiently capture the deformation in either pattern projected by E_p1 or E_p2 at points occurring either between α_1 and β_1 (or within α_1 and β_1 , α_1 and β_1 where the patterns don't mix) a method must be developed to distinguish between the patterns projected by E_p1 and E_p2 .

3. ALGORITHM FOR DETERMINING THE DEFORMATION

3.1 Algorithm Overview

This paper proposes a method to determine the deformation x_d in a fringe pattern within interfering fringe patterns by projecting orthogonal fringes from projectors E_p1 and E_p2 . Figure 2 shows a block diagram of the process.

3.2 Image Acquisition and Pre-Processing

Once the patterns are projected onto the object, an image is taken with an off the shelf CCD camera and transferred to the computer. When the image is loaded it is converted to a 256-bit grey-scale bitmap with pixel intensity values between 0 and 255. As the UPF measurement function takes values between -1 and 1 the image must be rescaled using the function

$$f(x) = \left(\frac{x - X_{max}}{X_{max} - X_{min}} \right) (upper - lower) \quad (1)$$

where X_{max} and X_{min} are the maximum and minimum values of the data vector $X \ni x$, and *upper* and *lower* are the desired scale range.

3.2. Locate Fringe Border

In general, when the fringes are projected onto the background and object the position of the projectors relative to the camera means

Difference between Median Filtered Image and Unfiltered Image

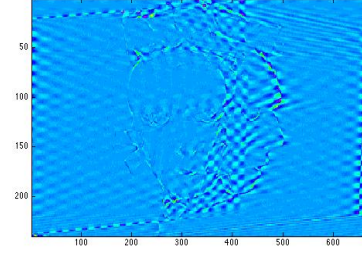


Fig. 3. Difference between median filtered and unfiltered image. The area where the interfering fringe is filtered can be seen in the middle

the fringe border will not be parallel to the edges of the image taken by the camera. As the pixel offset affects the accuracy of the estimation a straight line along the fringe border needs to be determined. Bresenham's line algorithm is used to achieve this. Section 6.3 details the effect of pixel offset on measurement accuracy.

3.3 Filtering Out The Undesired Fringe

To isolate the desired fringe it is first transformed to the frequency domain via 2-D FFT, and the undesired fringe filtered out. This is achieved simply by zeroing the peak of the undesired fringe in the frequency domain.

3.4 Median Filtering

The filtering process is unable to filter the undesired fringe in its entirety without also filtering some of the high frequency components of the desired fringe. This leads to some interference between the two fringes. A row or column wise median filter is used in the image depending on whether the desired fringe is vertical (column) or horizontal (row). This process evens out the fringes and reduces interference from the undesired fringe. Fig. 3 shows the difference between an image that has been filtered with a 10x1 row-wise median filter and an unfiltered image.

3.5 Determining The Object Deformation

Once the desired fringe has been isolated the resulting image is scanned on a line-by-line basis and the deformation in the fringe pattern due to the object is determined. Each line of the fringe pattern is essentially a phase modulated cosine wave, with the change in phase due to the deformation in the pattern caused by the object.

3.5.1. Cosine Fringe Pattern Model

A single line of a filtered fringe pattern can be modeled as a phase modulated cosine wave that can be represented as:

$$f(x_n) = B + a(x_n) \cos(2\pi f_c x_n + \phi(x_n)) \quad (2)$$

$$n = 1, 2, 3 \dots N$$

where x_n represents the pixel number in the x direction of an $N \times M$ size grey scale image $a(x_n)$ is the fringe amplitude, f is the fringe centre frequency, and $\phi(x_n)$ is the phase (for a horizontal fringe the scan direction would be in the y_m direction). The pixel wise shift in the pattern occurs when the fringe is projected onto the reference plane at point B and reflected to the camera E_c . When the reference plane is removed the pattern is reflected to the object onto point H and is reflected to the camera through point B, which occurs in a shift in the fringe pattern due to the object, denoted as x_d in Fig. 1. This shift in the fringe pattern can be modeled as a modulation in the phase of the fringe. For example taking the line of the fringe pattern in the x (horizontal) direction:

$$\begin{aligned} g(x_n) &= f(x_n, y_m) \\ g(x_n) &= B + a(x_n) \cos(2\pi f_c x_n + \phi(x_n, x_d)) \\ g(x_n) &= B + a(x_n) \cos(2\pi f_c x_n - u(x_d)) \end{aligned} \quad (3)$$

where $u(x_d) = -x_d/2\pi f_c$ represents the pixel wise shift in the fringe pattern due to the object. The variable to estimate is the deformation $u(x_d)$ and can be done via a non-linear filter such as the UPF. For this procedure the state function consists of returning the deformation estimate scaled by a transition matrix:

$$u(x_n) = \phi_u u(x_{n-1}) + v_u(x_n) \quad (4)$$

where ϕ_u is the 1×1 transition matrix, $v_u(x_n)$ is an AWGN noise parameters with variance σ_u^2 . The model function returns a modified equation 2:

$$h(x_n) = \cos(2\pi f_c x_n - u(x_n)) \quad (5)$$

3.5.2. Unscented Particle Filter

The Unscented Particle Filter [15] is a Sequential Monte Carlo technique for non-linear state estimation which uses the Unscented Kalman Filter as an importance proposal distribution in order to increase the accuracy of the filter. Some other methods for designing importance proposals include a simple prior consisting of the state transition (transition prior), auxiliary particle filtering, using the Extended Kalman Filter for the importance proposal. As the state transition for this system simply returns current deformation estimate the transition prior is unsuitable as an importance proposal. The EKF linearises a non-linear function and does not give as accurate an estimate as the UKF, and the APF does not necessarily guarantee an improvement over the normal PF in all circumstances.

The UKF was first introduced in [16] and is a method to estimate a given state vector from a nonlinear observation model. The UKF operates around the unscented transform which is a method for estimating the mean and covariance of a random variable [17]. For a complete description of the UKF the interested reader is referred to [16] [17] and the references therein.

One of the most critical steps in the particle filter is the calculation of an adequate proposal distribution [15, 18]. To this end the UKF is used to first estimate the state vector and then the particle filter is used to estimate the state mean. For a detailed treatment of the UPF see [15].

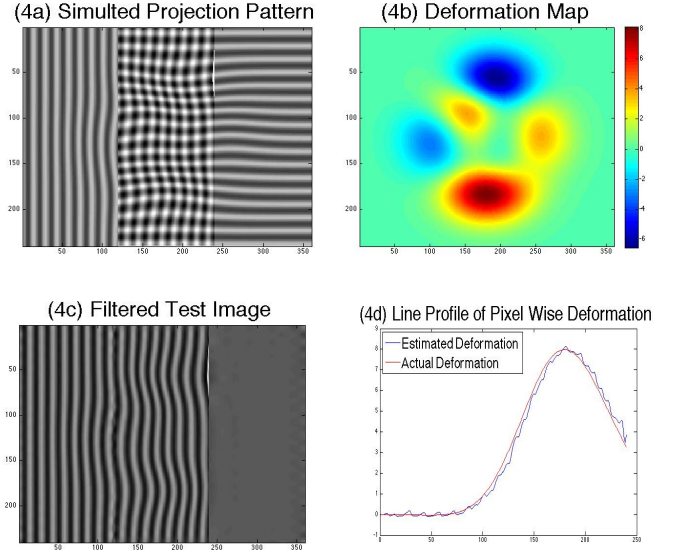


FIG. 4. Simulation results of the multi-projector profilometry system

5. SIMULATION AND EXPERIMENTAL RESULTS

The simulation pattern is shown in figure 4a, with the deformation shown in figure 4b, and the filtered pattern in 4c. The test deformation is determined in 2 dimensions by:

$$\varphi(x_n, y_m) = 3(1 - x_n)^2 \exp(-x_n^2 - (y_m + 1)^2) - 10 \left(\frac{x_n}{5} - x_n^3 - y_n^5 \right) \exp(-x_n^2 - y_n^2) - \frac{1}{3} \exp(-(x + 1)^2 - y^2) \quad (6)$$

where x_n and y_m are the pixel number in the x and y direction and the height of the function corresponds to pixel shift and sub-pixel shifts were performed by a 2D spline interpolant. This is chosen as ground truth, or “ideal” deformation, which is the deformation to be determined by the UPF. Figure 4d shows a line profile between the ground truth and the UPF estimation. The parameters used for the UKF are $\alpha = 0.0025$, $\beta = 2$, $\kappa = 0$, the process noise $Q_k = 0.6 * 10^{-2}$, and the measurement noise $\mathcal{R}_k = 0.008$, and posterior covariance noise $\sigma = 0.5$. For real world tests, two blank white facemasks were chosen for the test objects. These were used because they have no surface texture to interfere with the fringe and the shape of a face was deemed a suitably complex shape to test the algorithm. The object was placed on a projector screen and the fringe patterns projected via an off the shelf Panasonic PT-AE7500 projector, and the images were captured with a Nikon Coolpix S6300 (Fig. 5a). Fig. 5b shows the left side of the projected pattern, and 5c shows the estimated object shape. The new parameters in this scenario are increased measurement noise $\mathcal{R}_k = 0.3$, and $Q_k = 0.1$ and covariance of $\sigma = 0.1$.

6. DISCUSSION

Figure 4a shows the simulated test pattern with overlapping fringes in vertical and horizontal direction. The image is constructed by first overlapping the images and then applying the deformation.

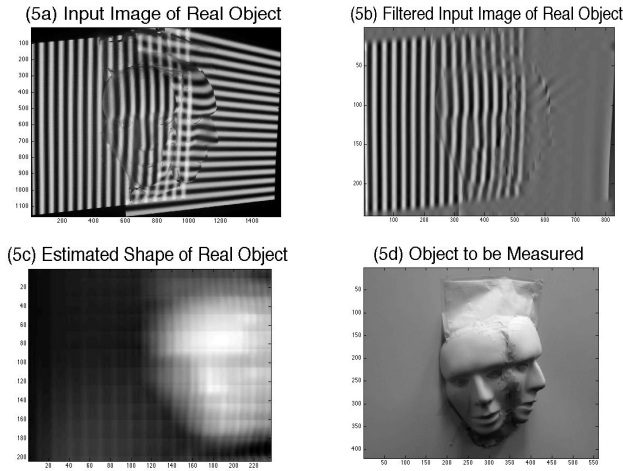


FIG. 5. Real object test of the multi-projector profilometry System

Figure 4c shows the test image with just the vertical fringe. The amplitude of the fringes is reduced in the filtering process making the fringe pattern darker than the unfiltered image, although this does not have an effect on the estimation. Figure 4d shows the estimation from the UPF, with the true deformation in red and estimation in blue. There is some distortion in the estimation, which is due to the level of the UPF parameters. Although decreasing the process noise and increasing the measurement noise of the UPF can mitigate this, it has the trade off of a decrease in measurement accuracy. Figure 5a shows the input multi-fringe image of the real world object (Fig. 5d). Figure 5b shows the input image after filtering out the horizontal fringe and applying a 10x1 median filter to reduce the interference of any overlapping horizontal fringe that wasn't fully filtered out. The median filtering process acts as a smoothing filter; consequently some of the high frequency components of the desired fringe are removed resulting in a loss of detail, although this may be able to be reduced by a suitable image super-resolution technique. Figure 5c shows the estimated shape of the single mask object from figure 5b.

6.1 Error Sources

Two of the major error sources in the estimate are the pixel offset of the input fringe pattern and amplitude of the cosine fringe pattern.

6.1.1 Pixel Offset Error

Figure 6a shows the effects of pixel offset to the measurement accuracy, with the mean square error between the estimation of the UPF and the ground truth with increasing pixel offset. The pixel-offset error is analogous to phase offset error, and arises when the start pixel for the line scanning algorithm causes the initial phase of the input cosine to be different from what the model requires. The cause of this is due to the projector setup projecting the fringe pattern such that the fringe boundaries are not parallel to the borders of the input image. The proposed solution in this paper is to first manually select the start points of the image and then approximate a straight line along the fringe border using

Bresenham's line algorithm. Fig 6b shows the results of this procedure. The red line in the image is the

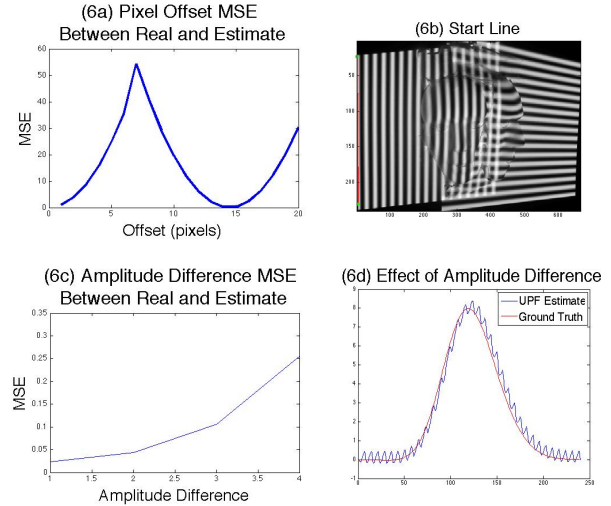


FIG. 6. (6a) MSE Between Estimate And Ground Truth For UPF (6b) Proposed Solution Using Bresenham's Line Algorithm (6c) Amplitude Difference Error (6d) Effect Of Incorrect Amplitude On Parameter Estimate

straight line approximation which serves as the start point for each scan line.

6.1.2 Amplitude Difference Error

The second major source of error arises from the difference between the input cosine fringe and the amplitude of the fringe required by the model. Fig. 6c shows the MSE between the estimate and the ground truth simulation with increasing amplitude difference. This sort of error results in periodic noise of the type seen in Fig. 6d and Fig. 5c. Decreasing the process noise for the UPF could mitigate the effect of amplitude difference, however this will also decrease the level of detail detected by the UPF.

7. CONCLUSION

In this paper a method for multi-view object detection using a single image and multiple projectors was presented. One of the limitations with single projector one-shot profilometry algorithms is the inability to image the entire shape at once. This limitation was addressed by the use of multiple grey-scale sinusoidal fringe patterns projected at right angles to each other, which are filtered out in the frequency domain before the resulting fringe pattern is demodulated using an Unscented Particle Filter. A Bayesian filtering scheme (Unscented Particle Filter) was used to demodulate the fringe pattern and retrieve the object shape. Two major error sources present with the proposed Bayesian approach were also discussed. The Pixel offset error of the input scan line was addressed by the use of Bresenham's line algorithm, which approximated a straight line along the fringe boundary. It was also shown that the amplitude difference between the input cosine and the model amplitude resulted in periodic noise. Future work will examine improved fringe isolation methods that do not filter out the high frequency components of the desired fringe. Also an automated way of detecting the start point for the input fringe and

methods to reduce the error caused by amplitude difference between the input scan line and the required model amplitude.

8. REFERENCES

- [1] P. Zheng, H. Guo, Y. Yu, and M. Chen, "Three-dimensional profile measurement using a flexible new multi-view connection method," 2008.
- [2] H. Guo and M. Chen, "Multiview connection technique for 360-deg three-dimensional measurement," *Optical Engineering*, vol. 42, pp. 900-905, // 2003.
- [3] H. He, M. Chen, H. Guo, and Y. Yu, "Novel multiview connection method based on virtual cylinder for 3-D surface measurement," *Optical Engineering*, vol. 44, // 2005.
- [4] R. Furukawa, R. Sagawa, H. Kawasaki, K. Sakashita, Y. Yagi, and N. Asada, "Entire shape acquisition technique using multiple projectors and cameras with parallel pattern projection," *IPSI Transactions on Computer Vision and Applications*, vol. 4, pp. 40-52, // 2012.
- [5] R. Furukawa, R. Sagawa, H. Kawasaki, K. Sakashita, Y. Yagi, and N. Asada, "One-shot Entire Shape Acquisition Method Using Multiple Projectors and Cameras," in *Image and Video Technology (PSIVT), 2010 Fourth Pacific-Rim Symposium on*, 2010, pp. 107-114.
- [6] Y. Cai and X. Su, "Inverse projected-fringe technique based on multi projectors," *Optics and Lasers in Engineering*, vol. 45, pp. 1028-1034, // 2007.
- [7] O. A. Skydan, M. J. Lalor, and D. R. Burton, "New technique for phase measurement and surface reconstruction using coloured structured light," ed, 2002, pp. 277-282.
- [8] O. A. Skydan, M. J. Lalor, and D. R. Burton, "Using coloured structured light in 3-D surface measurement," *Optics and Lasers in Engineering*, vol. 43, pp. 65-78, // 2005.
- [9] J. Villa, M. Servin, and L. Castillo, "Profilometry for the measurement of 3-D object shapes based on regularized filters," *Optics Communications*, vol. 161, pp. 13-18, 3/1/ 1999.
- [10] I. Gurov, E. Ermolaeva, and A. Zakharov, "Analysis of low-coherence interference fringes by the Kalman filtering method," *Journal of the Optical Society of America A: Optics and Image Science, and Vision*, vol. 21, pp. 242-251, 2004.
- [11] I. Gurov, M. Volynsky, and E. Vorobeva, "Dynamic wavefront evaluation in phase shifting interferometry based on recurrence fringe processing," 2010, pp. 479-484.
- [12] I. Gurov and M. Volynsky, "Interference fringe analysis based on recurrence computational algorithms," *Optics and Lasers in Engineering*, vol. 50, pp. 514-521, 2012.
- [13] I. P. Gurov and D. V. Sheynihovich, "Interferometric data analysis based on Markov nonlinear filtering methodology," *Journal of the Optical Society of America A: Optics and Image Science, and Vision*, vol. 17, pp. 21-27, 2000.
- [14] T. E. Zander, V. Madyastha, A. Patil, P. Rastogi, and L. M. Reindl, "Phase-step estimation in interferometry via an unscented Kalman filter," *Optics Letters*, vol. 34, pp. 1396-1398, 2009.
- [15] R. van der Merwe, N. de Freitas, A. Doucet, and E. Wan, "The Unscented Particle Filter," in *Advances in Neural Information Processing Systems 13*, 2001.
- [16] E. A. Wan and R. van der Merwe, "The Unscented Kalman Filter," in *Kalman Filtering and Neural Networks*, ed: John Wiley & Sons, Inc., 2002, pp. 221-280.
- [17] S. Julier, J. Uhlmann, and H. F. Durrant-Whyte, "A new method for the nonlinear transformation of means and covariances in filters and estimators," *IEEE Transactions on Automatic Control*, vol. 45, pp. 477-482, 2000.
- [18] R. Yong and C. Yunqiang, "Better proposal distributions: object tracking using unscented particle filter," in *Computer Vision and Pattern Recognition, 2001. CVPR 2001. Proceedings of the 2001 IEEE Computer Society Conference on*, 2001, pp. II-786-II-793 vol.2.